Anti-loosening mechanism of pitch difference bolt nut connections based on Junker loosening test

Nao-Aki Noda, Biao Wang, Yoshikazu Sano, Ryo Kawano, Yuto Inui, Xi Liu & Yasushi Takase

Taylor & Francis
Taylor & Francis Group

Check for updates

Anti-loosening mechanism of pitch difference bolt nut connections based on Junker loosening test

Nao-Aki Noda[a], Biao Wang[b], Yoshikazu Sano[a], Ryo Kawano[a], Yuto Inui[a], Xi Liu[c], and Yasushi Takase[a]

[a]Mechanical Engineering Department, Kyushu Institute of Technology, Kitakyushu-city, Japan; [b]School of Aerospace Engineering and Applied Mechanics, Tongji University, Yangpu, Shanghai, China; [c]School of Mechanical Engineering, Yanshan University, Qinhuangdao, Hebei, China

ABSTRACT

Bolt nut connections are essential elements and widely used in industry. The authors have verified that introducing a slight pitch difference between the bolt and the nut may improve the anti-loosening performance and fatigue life of the bolt nut connections. Besides, the effect of residual torque of pitch difference bolt-nut connections on the loosening resistance performance was discussed. In this study, the Junker loosening test was investigated experimentally and analytically to confirm the anti-loosening performance of pitch difference bolt nut connections directly. The FEA results are in good agreement with the experiments. It is confirmed that, for pitch difference bolt nut connections, the threads contact status is different from the common bolt nut connections, and the torque between the thread contact surface friction is the main reason of anti-loosening performance improvement of the pitch difference bolt nut connections. In addition, the results showed that if the pitch difference is large enough, the nut loosening angle equals the tightening angle for each vibration, and nut loosening does not occur. If the pitch difference is relatively small but just large enough to provide a prevailing torque, with increasing of the vibrations number of the nut, the loosening speed decreases gradually and finally the clamping force remains steady, which means the bolt nut connections retain anti-loosening performance to some extent.

1. Introduction

Bolt-nut connections are standardized mechanical elements that are frequently and widely used in the industry due to their low cost and ease of maintenance. For example, there are about 3000 bolt-nut connections used in one automobile. Loosening failure of the bolt-nut connections may cause the failure of structures and even disasters. Until now, loosening failure of bolt-nut connections has still been a big problem for industries. Therefore, many researchers focused on the loosening resistance performance of bolt-nut connections (Chen, Shimizu, and Masuda 2012; Izumi et al. 2009; Liu, Gong, and Ding 2018; Noda et al. 2008a, 2008b; Ranjan, Vikranth, and Ghosal 2013; B. Yang et al. 2021; L. Yang et al. 2021; You et al. 2020; Zhang et al. 2018; Zhou et al. 2018).

There are mainly two methods widely used for preventing nut loosening. One is to use special washers, and the other is to change the shape of the nuts (Bhattacharya, Sen, and Das 2010; Gong, Liu, and Feng 2022; Panja and Das 2016, 2017; Samanta et al. 2012). Sawa et al. conducted a series of Junker loosening experiments by varying washers with M12 nut shapes (Sawa, Ishimura, and Yamanaka 2006; Shoji, Sawa, and Yamanaka 2007). It was found that loosening prevention performance was improved by using plate washers, spring washers, toothed washers, and Nord lock washers compared to normal bolt-nut connections without them. Like a washer, a flange nut has a wide flange surface at the bearing nut side, usually with a serrated shape, which contributes to anti-loosening. It was reported that 110 percent of the tightening torque is required to loosen the flange nut (Barrett 1990). Flange nuts are mainly used for wood and plastic. Slotted nut, also known as Castle Nut, has some slots on the free nut end side, and they are usually used together with a pin. This type of nuts is suitable for situations when the initial tightening torque needed is small (Barrett 1990). Super lock nut (SLN) is a kind of wire inserted nut and is widely used in industries such as transportation and bridges provided by Fuji Seimitsu Co. Different from the common nut, this type of nut can be reused several times. Since a spring is inserted in the thread, the loosening energy can be absorbed and transferred to a locking torque when vibrating the bolted joints.

Except for the special nut shapes mentioned above, prevailing torque-type nuts are widely used for anti-loosening (Eccles, Sherrington, and Arnell 2010; Eccles 2010). Daiki industry and Tokyo university developed the Super Slit Nut (SSN), whose slit provides a suitable pitch difference by pressing the upper part of the nut to be deformed. The experimental study with FEM analysis for JIS M12 SSN showed the prevailing torque $T_P = 15-19$ Nm contributing to superior anti-loosening performance (Izumi et al. 2005b). Nishiyama et al. designed a kind of nut named Hyper Lock Nut (HLN) whose shape is similar to SSN (Nishiyama et al. 2009). Although both of the nuts have a cut portion, in HLN, instead of pressing the thinner nut part to be deformed by the press, a very small part of the bearing surface side of the nut is cut, and the included angle of the cutting surface and the bearing surface is 1 degree. HLN can provide good anti-loosening performance without a complicated tightening process. Gong et al. designed a kind with nut novel anti-loosening structure (Gong, Liu, and Ding 2021). For the newly proposed thread structure, both internal and external threads are changed, and it is considered that the modified thread shape can effectively inhibit relative sliding along the radial direction. The Junker test results showed that the axial clamping force even became slightly larger than the initial one after the vibration test. Wakabayashi designed a nut pair with an upper nut and a lower nut that eccentrically engage with each other to avoid loosening, named Hard Lock. This kind of bolt nut connection has witnessed the success of the Japan Shinkansen for several decades (Wakabayashi 2002). For many special anti-loosening nuts, multiple parts, and special shapes or geometries are needed, leading to a complex manufacturing process and high cost (Gong, Liu, and Ding 2021; Nishiyama et al. 2009; Wakabayashi 2002). Besides, there are also several researches on the improvement of fatigue strength of bolt nut connections (Hirai and Uno 2005; Majzoobi, Farrahi, and Habibi 2005; Noda, Xiao, and Kuhara 2011; Sawa et al. 2015).

Bolt nut connections with pitch differences were proposed as a technique for improving fatigue resistance and loosening resistance at low-cost many years ago, but no research was found to prove this. Therefore, in the previous papers (Chen et al. 2016; Noda et al. 2016, 2021; Xin et al. 2015), the authors experimentally verified that the anti-loosening performance and fatigue life could be improved by providing an appropriate pitch difference between the nut and the bolt. The authors also indicated that the prevailing torque in the nut screwing process is closely related to the loosening resistance property (Chen et al. 2016; Noda et al. 2016). Furthermore, by applying a 3D FEM to the nut loosening process where torque is applied in the loosening direction, the loosening resistance was discussed experimentally and analytically. Then, those screwing, tightening and untightening processes were expressed in terms of the $F\text{-}T$ relation (clamping force F vs. tightening torque T) (Liu et al. 2021; Noda et al. 2020, 2022; Wang et al. 2021). However, the effect of the pitch difference on the loosening resistance has not been clarified yet so far under real operating conditions.

Therefore, instead of "the untightening process in the *F-T* relation", this paper considers the Junker loosening test as "the loosening process in an *F-n* relation (clamping force *F* vs. vibration cycles *n*)". Then, the *F-n* relation will be clarified by comparing a 3D FEM analysis with a Junker loosening experiment, which is common and reliable method for testing and comparing the security of bolt nut connections (Pai and Hess 2002, 2004). Especially when the nut is subjected to a large number of vibrations, FEM simulation will be performed considering the specifications in the DIN standard demonstrating anti-loosening ability. This is to clarify the loosening/anti-loosening mechanism since the real nut loosening usually occurs when the nut is subjected to a large number of vibration cycles. Also, the present *F-n* relation will be studied by comparing it with the previous *F-T* relation. To clarify the nut loosening/anti-loosening mechanism, the θ_L-*n* relation (loosening angle θ_L vs. vibration cycle *n*) will also be newly investigated through the FEM simulation.

2. Experimental method and results for Junker loosening test

2.1. Loosening process in Junker test vs. untightening process

Figure 1 illustrates four stages of the nut in usage (a) screwing, (b) tightening, (c) loosening, and (d) untightening. As shown in Fig. 1(c), this paper mainly concerns the loosening process in the Junker loosening test under transverse loading after the nut tightening. In the loosening process, the clamping force *F* decreases under transverse vibration applied to the clamped body. Since the untightening process in Fig. 1(d) has been discussed in the previous study (Noda et al. 2022), the loosening process in Fig. 1(c) will be discussed in this paper.

2.2. Specimens

JIS M12 normal coarse thread in Fig. 2 is considered in this study. Both pitch of the bolt and nut is p = 1750 μm. As shown in Fig. 2(b), for the pitch difference nuts, the nut pitch is α μm larger than the bolt pitch. In this study, the pitch differences used are α = 35, 40, 50 μm. The clearance in the axial direction is C_z = 59 μm between the bolt and nut threads. Figure 2(c) shows the contact state between the bolt and nut thread surface during the screwing process of a pitch
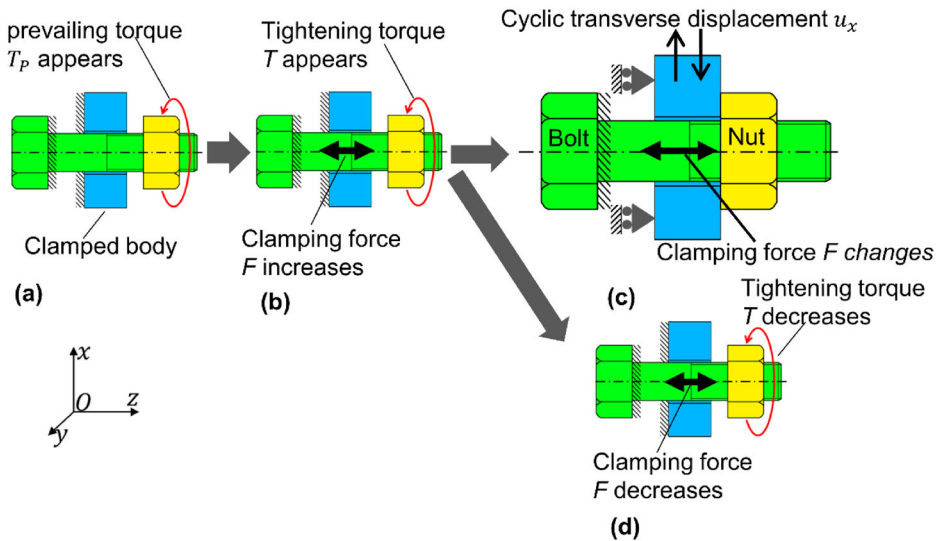

Figure 1. Schematic illustration for FEM modeling in (a) screwing process (b) tightening process (c) loosening process (d) untightening process.
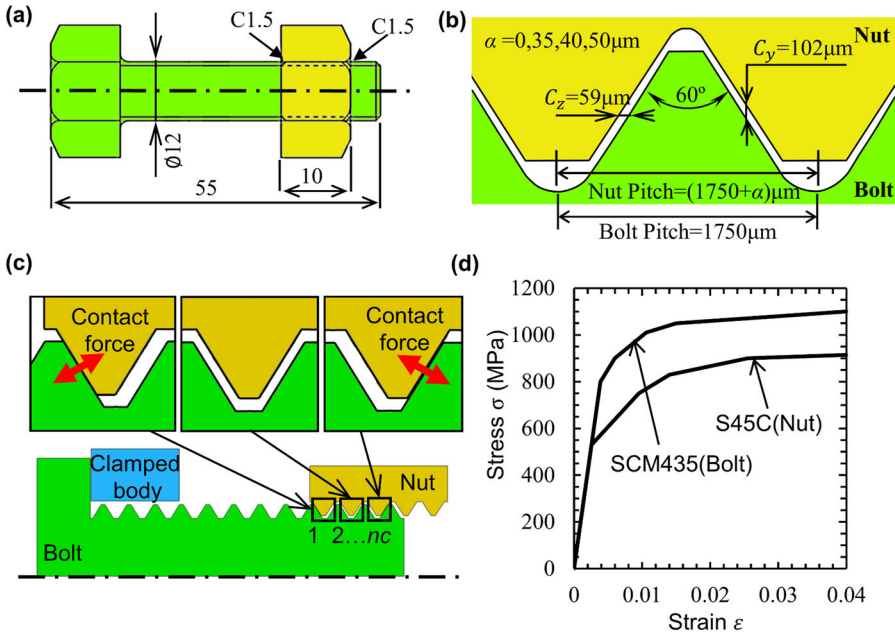
Figure 2. Dimension description (a) M12 Bolt-nut specimen [unit: mm]; (b) Pitch difference and clearance between bolt and nut threads [unit: μm]; (c) Pitch difference and clearance between bolt and nut threads [unit: μm].

difference nut. The bolts and the clamped body are made of Chromium-molybdenum steel SCM 435, for which the yield strength and tensile strength are 800 MPa and 1200 MP, respectively. The nuts are made of medium carbon steel S45C, for which the yield strength and tensile strength are 530 MPa and 980 MP respectively. The constitutive models of the materials are shown in Fig. 2(d). Both the bolt and the nut are made by cutting with the manufacturing error within 3 μm.

2.3. Experimental method

Figure 3(a) shows the Junker testing machine used for the loosening tests belonging to Fuji Semitsu Co., Ltd. Figure 3(b) is a schematic illustration of the main part. The movable plate is fastened to the fixed plate with bolts and nuts via rollers, and the initial clamping force before loosening is $F_{22.3}\% = 15$ kN. Since the movable plate is supported by rollers, the friction with the fixed plate can be ignored, as shown in Fig. 1(c). As shown in Fig. 2(c), before the whole nut is screwed onto the bolt, the prevailing torque T_p appears from the point the nut end threads contact, and T_p increases until the whole nut is screwed onto the bolt. During the loosening process, due to the rotation of the eccentric shaft in Fig. 3(a) at a frequency of 8 Hz, the moveable plate (the clamped body in Fig. 1c) vibrates in the transverse direction. The applied displacement $u_x = \pm 1mm$ in Fig. 3 is determined from DIN 65151 by loosening the normal nut $\alpha = 0$ as $F = 0$ (no clamping force) at $n = 300 \pm 100$. The revised DIN25201 prescribes no less than 80% of the initial clamping force at $n = 2000$ as the anti-loosening criterion. Instead, this study uses no less than 80% of the initial clamping force at $n = 1500$ for anti-loosening (HARDLOCK Industry Co. Ltd 2022).

2.4. Experimental results and discussion

2.4.1. F-n relation in Junker loosening test
Figure 4 shows the relationship between the clamping force F and the load cycle n experimentally obtained after starting the vibration test. The clamping force F was recorded three times in every
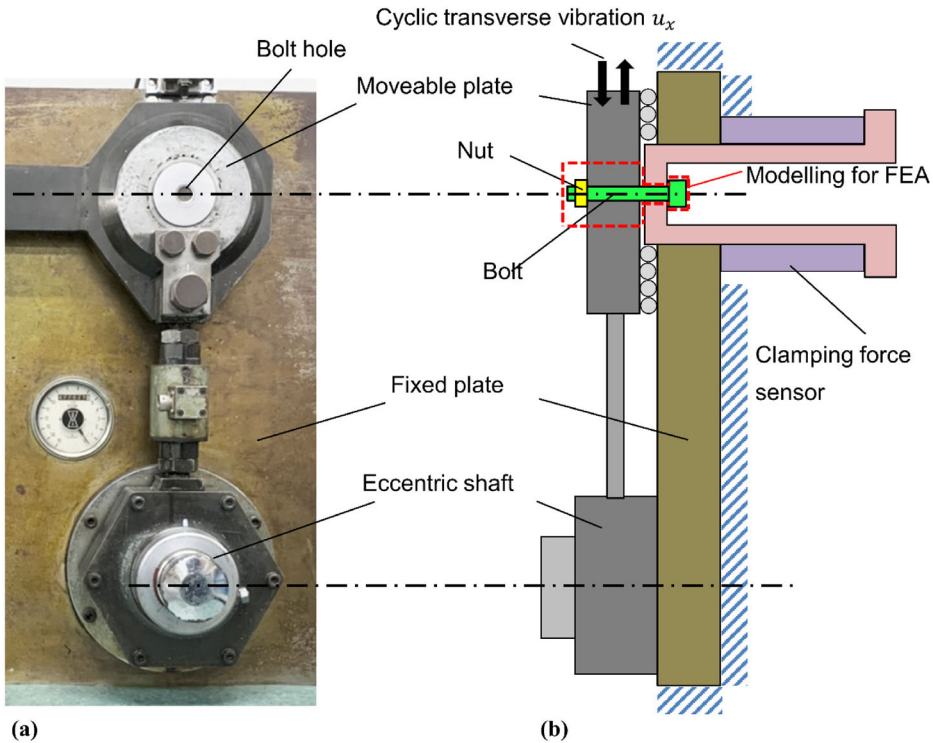
Figure 3. Junker loosening experimental device based on DIN 65151. (a) Photo of Junker's device; (b) schematic illustration.
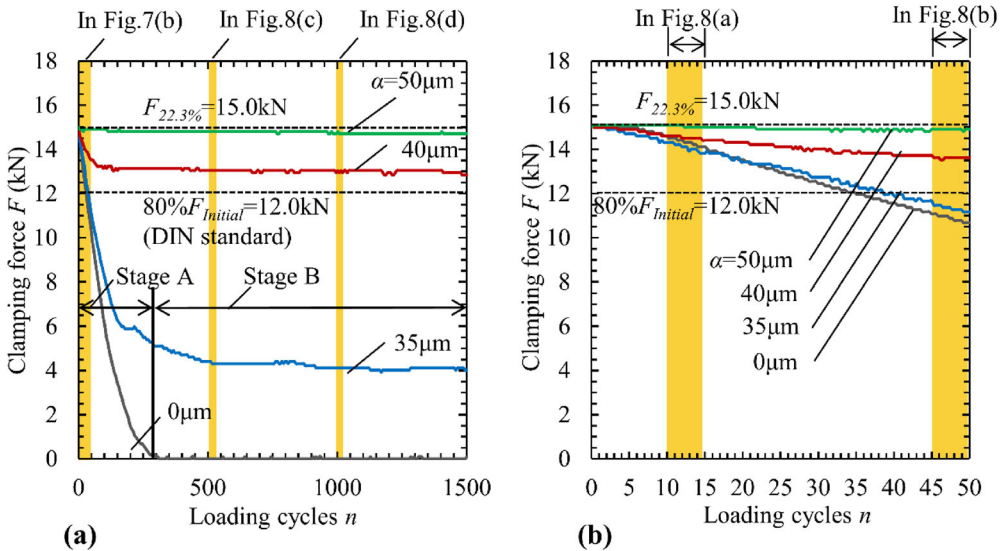
Figure 4. Experimentally results of the relation between clamping force F and loading cycles n. (a) 0–1500 cycles; (b) 0–50 cycles. (Stage A: Loosening progressing stage; Stage B: Loosening stopping stage).

vibration cycle. Since the experimental data is unstable in the early vibration stage ($n < 10$), the experimental results are considered for n $\geq$ 10. The initial clamping force was set as $F = 15\,\text{kN}$ before the vibration of the plate.

The F-n relations in Fig. 4(a) show that the reduction of the clamping force F becomes smaller for larger α. When α is large enough to generate the prevailing torque in the screwing process (Noda et al. 2016), the F-n relation can be classified into two stages. One is "the loosening progressing stage A" where the clamping force F decreases significantly, and the other is "the loosening stopping stage B" where the clamping force hardly decreases. For example, for $\alpha = 35\,\mu m$ in Fig. 4(a), a significant change can be seen for the decrease rate dF/dn around $n = 300$. Therefore, $n \leq 300$ can be regarded as stage A and $n \geq 300$ can be regarded as stage B.

As shown in Fig. 4(a), the experimental results showed that the pitch difference $\alpha = 40$–$50\,\mu m$ satisfies the DIN25201 anti-loosening standard prescribing that the residual clamping force F should be larger than 80% of the initial clamping force. Although $\alpha = 35\,\mu m$ does not satisfy the standard but sustains a certain amount of F. For example, when $n = 1500$, the residual clamping force $F = 4\,kN$ is 27% of the initial clamping force suggesting that $\alpha = 35\,\mu m$ has a virtual anti-loosening ability. The detail will be discussed in Sec. 3.3.

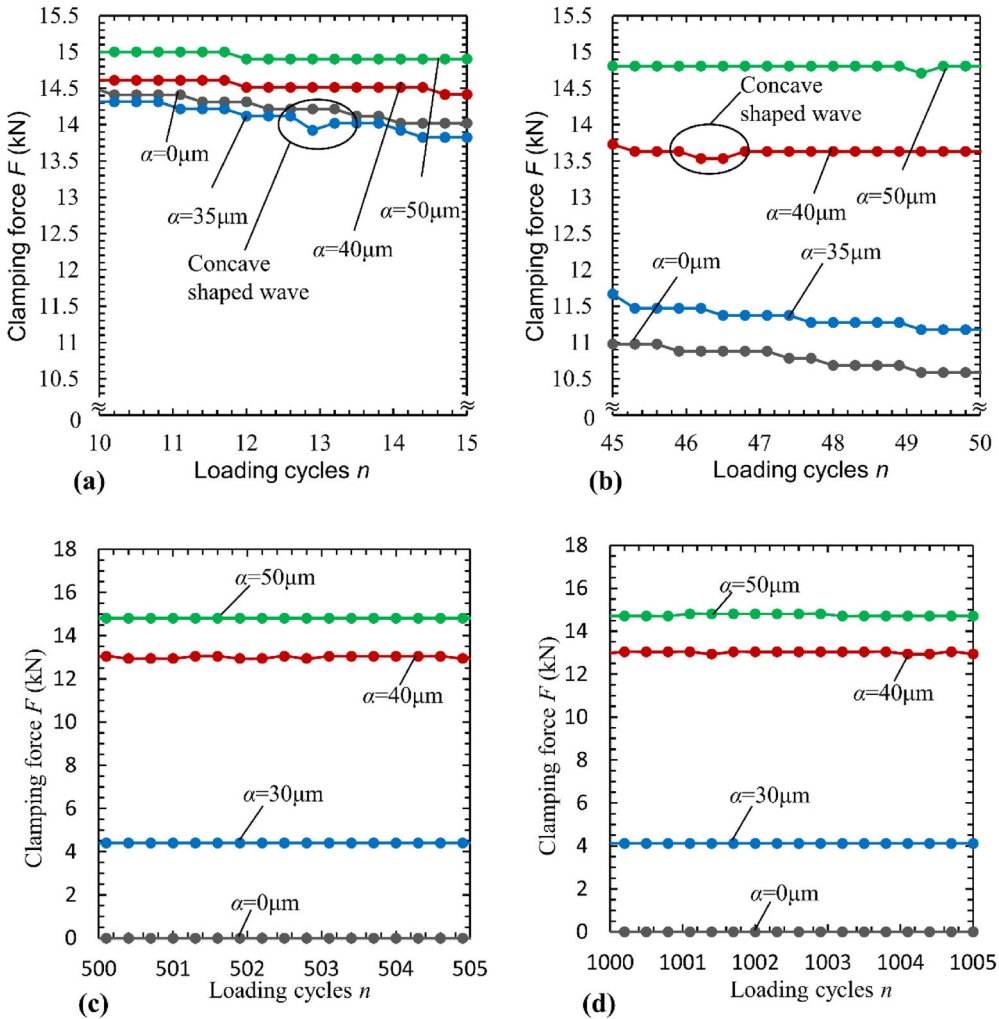Figure 5. Enlarged F-n relation to clarify the local variation of F. (a) $n = 10$–15 cycles; (b) $n = 45$–50 cycles; (c) $n = 500$–505 cycles; (d) $n = 1000$–1005 cycles. (Dotted point denotes where F is measured.).

2.4.2. Waveform in F-n relation in the loosening process

Figure 5 shows the enlarged *F-n* relation used to discuss the waveform. For example, Fig. 5(a) shows the *F-n* relation during $n = 10–15$. As shown in Figs. 5(a) and 5(b), when $\alpha = 0$, $35\,\mu$m, some waveforms of the lines occurred. However, when $\alpha = 40$, $50\,\mu$m, there is no waveform of the lines. Since the waveform of $n = 10 \sim 15$ in Fig. 5(a) is almost similar to the waveform of $n = 45 \sim 50$ in Fig. 5(b), the loosening progresses steadily after $n = 10$. The waveform becomes steadier during $n = 45–50$. For example, when $\alpha = 35\,\mu$m, three "step-like reduction waveforms" are seen during $n = 10 \sim 15$ in Fig. 5(a), but during $n = 45–50$ in Fig. 5(b), four "step-like reduction waveforms" were observed. Similarly, when $\alpha = 40\,\mu$m, and two "step-like reduction waveforms" are seen during $n = 10 \sim 15$ in Fig. 5(a), but during $n = 45–50$ in Fig. 5(b), a "step-like reduction waveforms" is observed.

Although the *F-n* relation of $\alpha = 35\,\mu$m is significantly decreasing during $n \leq 300$, as shown in Figs. 5(a) and 5(b), a "concave waveform" can be seen almost once every five cycles. Also, in the range other than Figs. 5(a) and 5(b), a "concave waveform" can be confirmed every five cycles for $\alpha = 35\,\mu$m. Instead, when $\alpha = 40\,\mu$m, one or two "concave waveforms" can be seen; and when $\alpha = 0$, no "concave waveforms" can be seen. The "concave waveform" in $\alpha = 35\,\mu$m as well as in $\alpha = 40\,\mu$m is the key to consider the anti-loosening mechanism since in $\alpha = 0$, no "concave waveform" can be seen. In other words, the "concave waveform" of $\alpha = 35\,\mu$m in the *F-n* relation during $n \leq 300$, "the loosening progressing stage A" suggests that the *F-n* relation becomes constant, as shown in Figs. 5(c) and 5(d) during $n > 300$, "the loosening stopping stage B".

3. FEM simulation for Junker loosening test to compare the experiment

3.1. Simulation method for nut loosening

To clarify the anti-loosening performance of the pitch difference nut, numerical simulation is also performed to obtain the *F-n* relation by FEA. The fastening part of the Junker loosening experiment in Fig. 3(b) is simplified, as shown in Fig. 6. As shown in Fig. 6(a), the hexagonal part of the bolt head and nut is replaced with a simplified cylindrical shape. The dimensions of the movable plate are $40 \times 40 \times 15mm$ (length $\times$ width $\times$ thickness). Here, 8-node elements are used for meshing, and the minimum mesh size is 0.048 mm. The total number of elements is about 8.0×10^4, and the number of nodes is about 15.1×10^4. The penalty method is used for the contact analysis, and the material's nonlinearity is considered. The thread friction coefficient $\mu_s = 0.12$ and the under-head friction coefficient factor $\mu_w = 0.17$ are applied as in the previous studies (Noda et al. 2022). The finite element method analysis software ANSYS Workbench 16.2 is used for this simulation.

In this analysis, the nut is tightened until the clamping force reaches $F = 15kN$ as in the experiments. During the tightening process, the bearing side of the bolt head and the opposite surface to the bearing surface of the clamped body are fixed, as shown in Fig. 6(b). To save the calculation time, the distance between the movable plate and the nut is set as 0.05 mm at the beginning of the analysis. After the clamping force F reaches to 15 kN, the boundary conditions are changed as shown in Fig. 6(c), and the clamped body is no longer fixed and becomes moveable in the x-direction. Here, the displacement u_x with the amplitude $u_x = \pm 1mm$ is provided as a sine wave similar to the experiment. In this simulation, each cycle is discretized into 20 steps. Then, the simulation is performed until n = 50, when the loosening process becomes stable.

Figure 6(d) illustrates the relation between the clamping force F and the tightening torque T obtained by FEM simulation. The details of *F-T* relations were discussed in the previous study as well as the prevailing torque $T_P (T_P \equiv \sup T$ when $F = 0)$ (Noda et al. 2022). It can be seen that the tightening torque T for $F_{22.3\%} = 15$ kN increases with increasing of the pitch difference α.
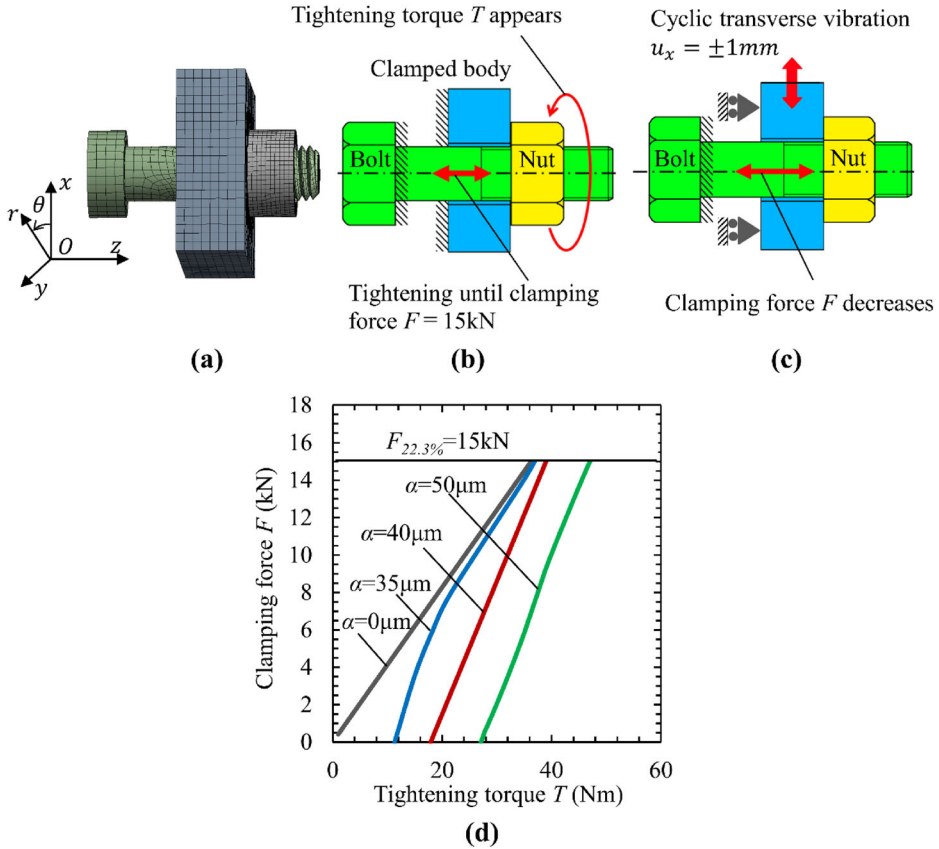
Figure 6. FEM model and boundary conditions for tightening process and loosening process. (a) FEM model; (b) Boundary conditions of tightening process; (c) Boundary conditions of loosening process due to transverse loading; (d) Clamping force F vs. tightening torque T during the tightening process.

3.2. F-n relation obtained by FEM to explain Junker loosening experiment

Figure 7 shows the F-n relation during $n \leq 50$ obtained by FEM simulation. Comparing Figs. 7(a) and 4(a), it can be found that the loosening order expressed by the slope dF/dn is the same, that is, $\alpha = 0 < \alpha = 35 \; \mu m < \alpha = 40 \; \mu m < \alpha = 50 \; \mu m$. As shown in Fig. 7(c), when $\alpha = 35 \; \mu m$, the "convex waveform" can be seen in FEM simulation immediately after the movable plate reaches a maximum displacement $u_x = 1mm$. Instead, as shown in Fig. 5(b), "step-like downward waveform" and "concave waveform" are observed in the experimental results different from Fig. 7(c). From Figs. 7(c) and 7(d), $\alpha = 35 \; \mu m$ and $\alpha = 40 \; \mu m$ have the same waveform when F changes immediately after the moveable plate reaches the peak values $u_x = \pm 1mm$. Instead, when $\alpha = 0$, the waveforms are totally different since $F \approx 0$. Although the waveforms of $\alpha = 35 \; \mu m$ and $\alpha = 40 \; \mu m$ are similar, the decreasing rate of F is totally different in stage A. The position of the maximum displacement and the position of "convex waveform" are expressed in the following Eqs. (1) and (2) independent of n by using the Gauss symbol $[n]$ to represent the integer part of the vibration cycle n.

$$\text{Position of the maximum } u_x : n - [n] = 0.25, \; 0.75. \tag{1}$$

$$\text{Position of the "convex waveform"} : n - [n] = 0.25 - 0.35, \; 0.75 - 0.85 \tag{2}$$

In Fig. 7, the anti-loosening mechanism of pitch difference nut can be clarified by comparing the waveforms of the standard nut $\alpha = 0$ with the one of $\alpha = 40 \; \mu m$, which satisfies the DIN anti-
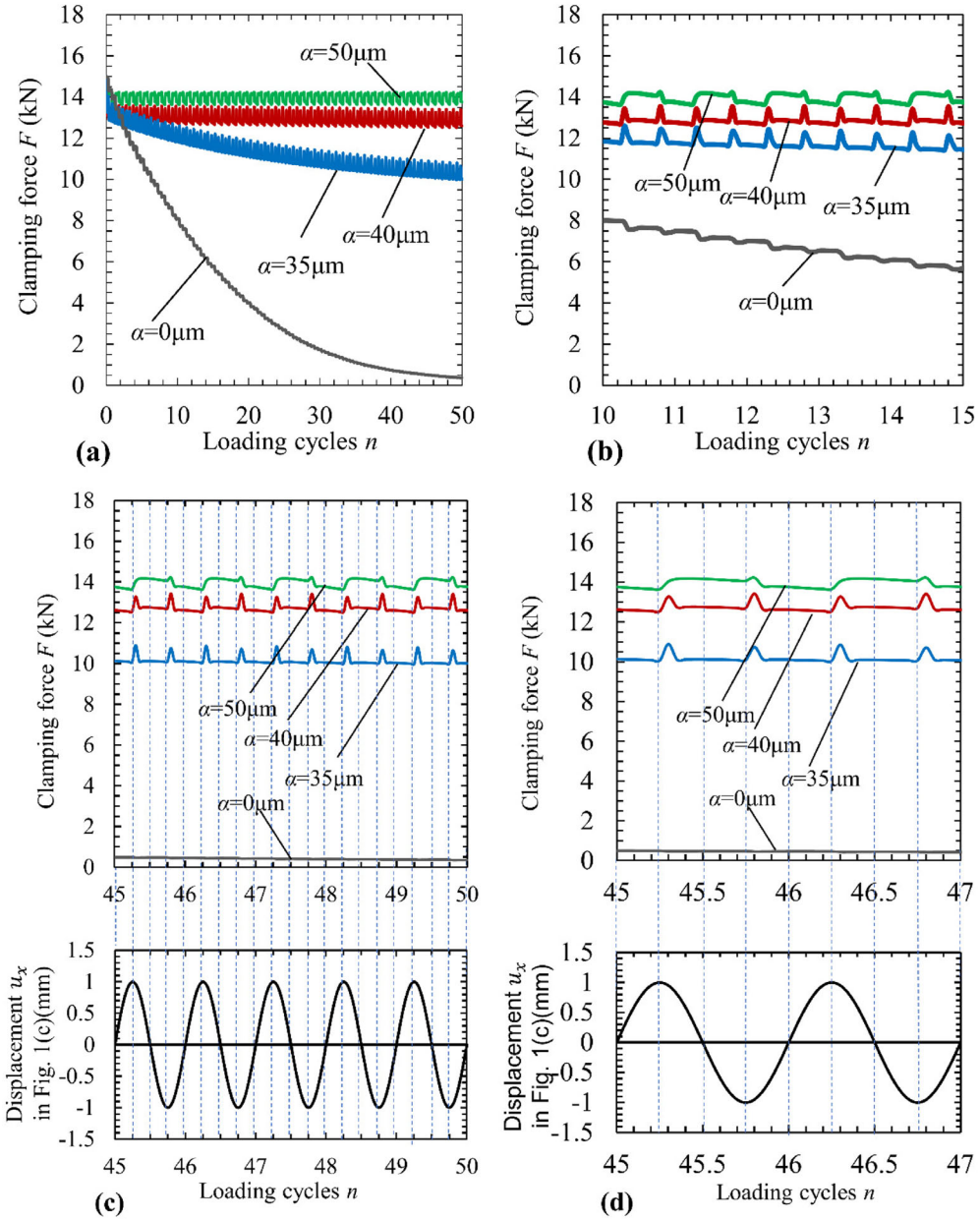
Figure 7. FEA relation between the clamping force F and loading cycles n. (a) n = 0–50 cycles; (b) n = 10–15 cycles; (c) n = 45–50 cycles; (d) n = 45–47 cycles.

loosening standard. Figures 8(a1)–(a4) illustrates the clamping force F and the bolt axial force F_α for $\alpha = 40\,\mu m$ in comparison with Figs. 8(b1)–(b4) for $\alpha = 0$. As indicated in Figs. 8(a1)–(a4), since both ends of the nut are in contact with the bolt thread due to the pitch difference, the bolt axial force $F_\alpha > 0$ appears (Noda et al. 2016). In Figs. 8(a1)–(a4), since the maximum displacement $u_x = 1mm \sim$ is applied to the nut with $\alpha = 40\mu m$ at $n = 45.25 \sim$, the clamping force F is changing as $F + \Delta F$. As shown in Fig. 7(d) at n = 45.25~, since the "convex waveform" appears, $\Delta F > 0$. Then, F_α is changing as $F_\alpha + \Delta F_\alpha$ with $\Delta F_\alpha < 0$. As shown in Figs.
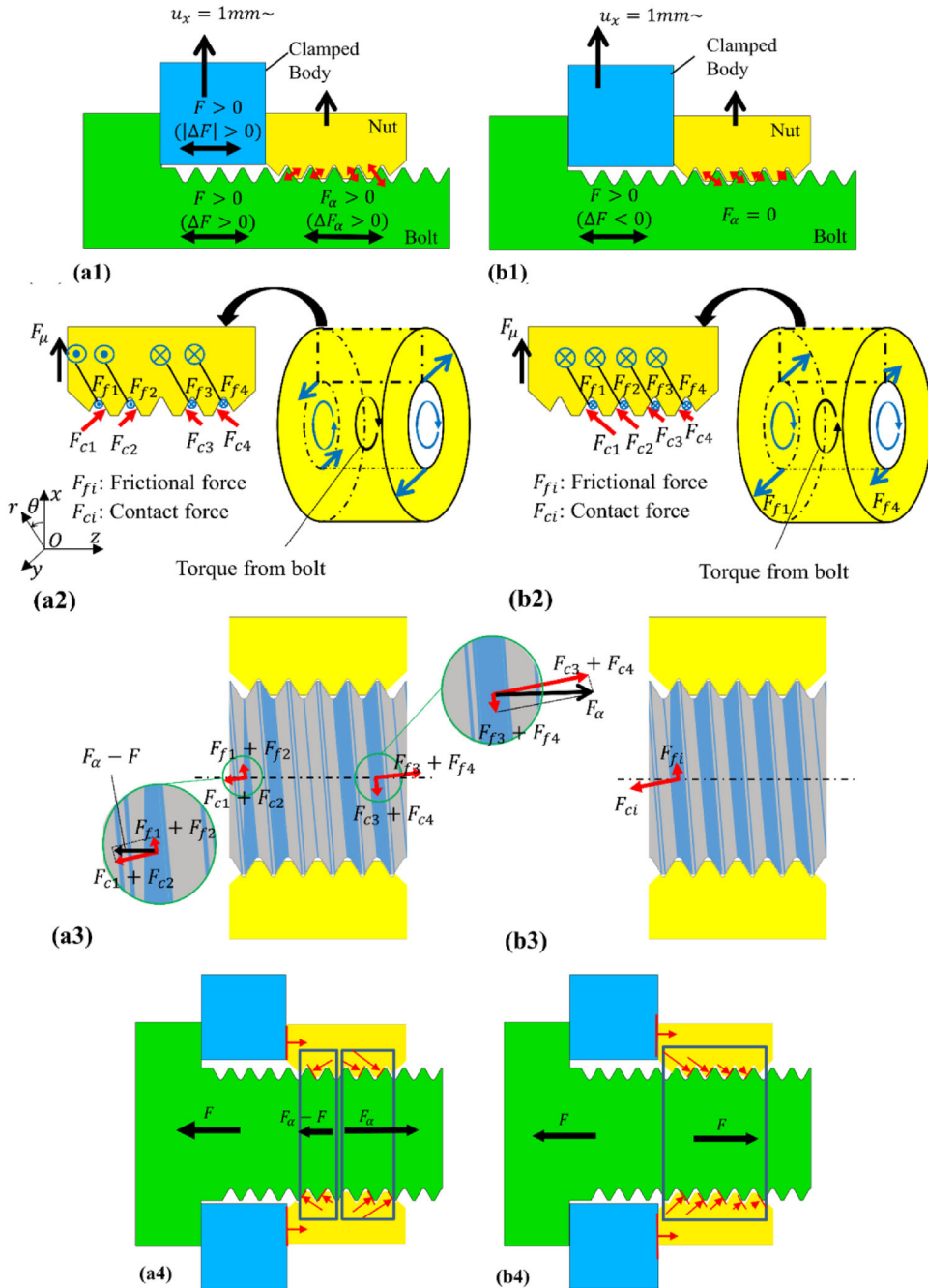
Figure 8. (a1) ΔF and ΔF_α due to $u_x = 1mm$ when $\alpha \geq 40\mu m$; (a2) Frictional force F_{fi} direction when $\alpha \geq 40\mu m$; (a3) Resultants $(F_\alpha - F)$ and F_α when $\alpha \geq 40\mu m$ (F_α denotes the bolt axial force due to the nut both ends contact); (a4) Bolt clamping force F and F_α which is the bolt axial force due to the nut both ends contact; (b1) ΔF due to $u_x = 1mm$ when $\alpha = 0$; (b2) Frictional force F_{fi} direction when $\alpha = 0$; (b3) Summation of resultants equal to F when $\alpha = 0$; (b4) Bolt clamping force F. (In (a1) and (b1), ΔF is the change of $F=$ the bolt clamping force F and ΔF_α is the change of $F_\alpha=$the bolt axial force due to the nut both ends contact; Here, $\Delta F=$change of bolt clamping force F, $\Delta F_\alpha=$change of the bolt axial force between the nut threads F_α due to the nut both ends contact).
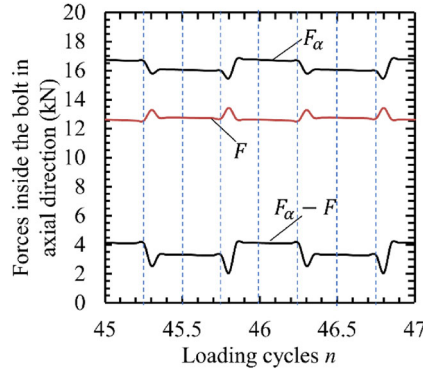
Figure 9. Variations of bolt axial force due to the nut both ends contact F_α (in Figure 8(a4)), clamping force F, and the resultant force of the left side part of the nut onto the bolt (F_α-F) (in Figure 8(a3)) for the loading cycle $n = 45$–47 of $\alpha = 40\ \mu$m.

Table 1. Frequency of concave/convex shape wave in F-n relation for n $= 10$–50.

	$\alpha = 0$	$\alpha = 35\ \mu m$	$\alpha = 40\ \mu m$
Experiments	×	△	△
FEM simulation	×	○	○

○: Always after peak in $|u_x|$, △: Sometimes, ×: Never

8(a1)–(a4), the direction of the thread contact force F_{c1}, F_{c2} in Fig. 8 are different from the ones of $\alpha = 0$. Due to the spiral of the threads, the directions of the frictional force F_{f1}, F_{f2} are also different. This is closely related to the appearance of the "convex waveform" in the simulation when $\alpha = =$ als

Figure 9 shows variations of the bolt axial force F_α, the clamping force F, and the difference between the two forces $(F_\alpha - F)$ during $n = 45$–47. As shown in Figs. 8(a3) and (a4), the bolt axial force F_α is produced as the resultant in the axial direction at the right side of the nut on the bolt thread $(F_{c3} + F_{c4})$ and $(F_{f3} + F_{f4})$. Similarly, $(F_\alpha - F)$ is the resultant force in the axial direction at the left side of the nut on the bolt thread $(F_{c1} + F_{c2})$ and $(F_{f1} + F_{f2})$. As shown in Fig. 9, it can be seen that after the displacement reaches the peak value $u_x = 1mm$ at n $= 45.25 \sim$, $(F_\alpha - F)$ decreases at first and then increases. Similarly, F_α decreases at first and then increases. However, since the value change of F_α is larger than the value change of $(F_\alpha - F)$, the "convex waveform" in the clamping force occurs.

As described above, the directions of the thread frictional forces F_{f1}, F_{f2} in Fig. 8(a3) at nut ends are different from the ones of $\alpha = 0$. That is to say, the anti-loosening torque is caused by $(F_{f3} + F_{f4})$, and the loosening torque is caused by $(F_{f1} + F_{f2})$. Since $(F_{f3} + F_{f4})$ is larger than $(F_{f1} + F_{f2})$, the whole torque due to frictional forces is acting in the anti-loosening direction. as a loosening resistance torque. During n $= 45.25$–45.3 in Fig. 9, since ΔF_α, is smaller than $\Delta(F_\alpha - F)$, $(F_{f1} + F_{f2})$ is smaller than $(F_{f3} + F_{f4})$. Consequently, since $\Delta(F_{f3} + F_{f4}) - \Delta(F_{f1} + F_{f2}) > 0$, the anti-loosening torque increases.

From the above discussion in Fig. 9, F_α, F, $(F_\alpha - F)$ take peak values at n $= 45.3$. As shown in Fig. 9, the decreasing rate of F_α is smaller than the decreasing rate of $(F_\alpha - F)$ when n $= 45.25$–45.3. Consequently, the decreasing rate of $(F_{f1} + F_{f2})$ is also smaller the decreasing rate that of $(F_{f3} + F_{f4})$. Since $\Delta(F_{f3} + F_{f4}) - \Delta(F_{f1} + F_{f2}) < 0$, the anti-loosening torque due to the friction increases. From Fig. 9, it can be seen that during n $= 45$–46, the value of $|(F_{f3} + F_{f4}) - (F_{f1} + F_{f2})|$ is almost constant. Therefore, except for the "convex waveform", the fastening force F does not change, and therefore, the nut hardly loosens.
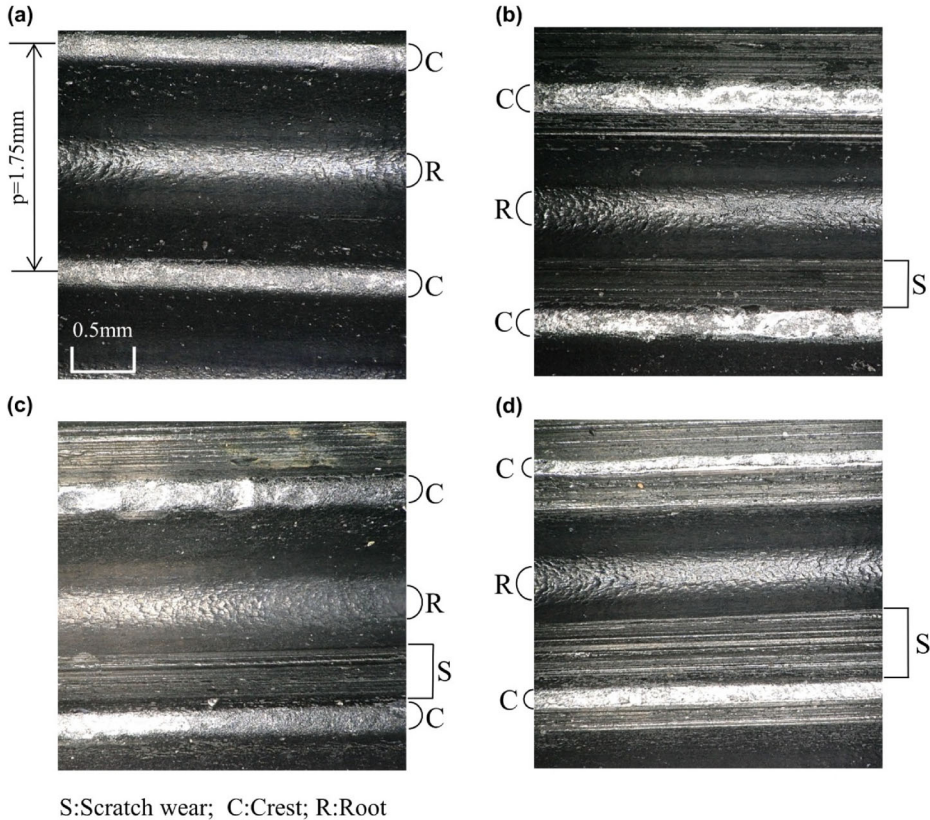
S:Scratch wear; C:Crest; R:Root

Figure 10. The thread surface of the bolt after the screwing in and screwing out process. (a) $\alpha = 0$; (a) $\alpha = 30\mu m$; (a) $\alpha = 40\mu m$; (a) $\alpha = 50\mu m$.

When $\alpha = 0$, the nut does not twist since only the thread surfaces opposite to the bearing side are in contact, and this is different from the situation when $\alpha = 40\,\mu m$. Therefore, the loosening resistance is small, and the vertical movement of the movable plate reduces the fastening force F and the nut loosens.

Table 1 summarizes the frequency of appearing the "concave/convex waveform" during $n = 10$–50 in the experiment in Fig. 4 and the FEM simulation in Fig. 7. Focusing on the experimental results in Table 1, the frequency of the concave waveform is 0–2 times in 5 repetitions for both $\alpha = 35\,\mu m$ and $\alpha = 40\,\mu m$ as denoted by $\triangle$: Sometimes in Table 1. Focusing on the FEM results in Table 1, a convex waveform is always observed after the peak of displacement for both $\alpha = 35\,\mu m$ and $\alpha = 40\,\mu m$ as denoted by $\bigcirc$: Always after peak in $|u_x|$ in Table 1. As shown in Table 1, $\alpha = 35\,\mu m$ and $\alpha = 40\,\mu m$ have a similar frequency of the "concave/convex waveform", $\alpha = 35\,\mu m$ may have a similar anti-loosening performance like $\alpha = 40\,\mu m$, which satisfies DIN standard. Instead, when $\alpha = 0$, such a "concave/convex waveform" cannot be observed suggesting that the anti-loosening performance is significantly inferior.

The difference of the waveforms between the FEM and the experiment can be explained from the change of the contacted thread surface conditions due to the wear and the generation of wear debris in the experiment. The bolt threads after the screwing in and screwing out process are shown in Fig. 10. The thread wear can be seen clearly for the pitch difference nuts. In the ANSYS FEM simulation, the friction coefficients between the threads cannot be changed and are assumed to be a constant value in the whole process (Noda et al. 2020).
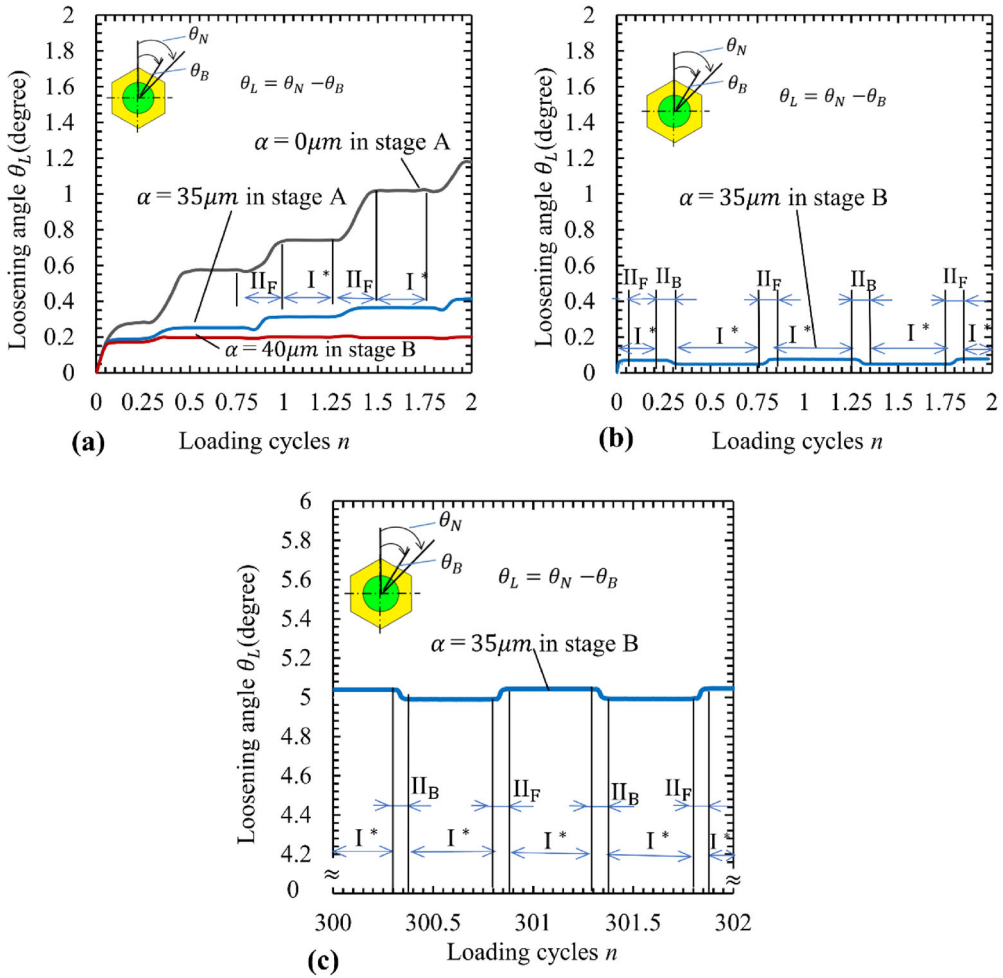
Figure 11. Nut loosening angles $\theta_L = \theta_N - \theta_B$ vs. loading cycles n. Here, θ_N = the nut rotation angle, θ_B = the bolt rotation angle, Stage A: Loosening process; Stage B: Loosening stop process. (a) Nut loosening angle θ_L when initial tightening force $F = 15$ kN for Stage A when $\alpha = 0, 35 \mu$m, Stage B when $\alpha = 40 \mu$m; Nut loosening angle θ_L when initial tightening force $F = 6$ kN in order to simulate Stage B when $\alpha = 35 \mu$m; (c) Nut loosening angle θ_L when initial tightening force $F = 15$ kN for Stage B when $\alpha = 35 \mu$m.

4. Fem simulation for nut loosening angle

4.1. Nut loosening angle θ_L versus vibration cycle n (θ_L-n relation) obtained by FEM simulation

Figure 11 shows the nut loosening angle θ_L vs. the vibration cycle n (θ_L - n relation) obtained by FEM simulation. The nut loosening angle θ_L can be defined $\theta_L = \theta_N - \theta_B$, where θ_N represents the nut rotation angle and θ_B represents the bolt rotation angle. Figure 11(a) illustrates the results for $n = 0$–2 after applying the initial clamping force $F = 15$ kN. It is seen that $\alpha = 40 \mu$m is in loosening stopping stage B and $\alpha = 0$ but $\alpha = 35 \mu$m are in loosening progressing stage A. To express stage B ($n > 300$) of $\alpha = 35 \mu$m with small calculation time, Fig. 11(b) shows the result for $n = 0$–2 after applying a fictitious initial clamping force $F = 6$ kN. To express stage B ($n > 300$) of $\alpha = 35 \mu$m by applying the real value $F = 15$ kN, Fig. 11(c) shows the result for $n = 300$–302, which can be obtained by using workstation HP Z440 (CPU E5-160 v4 @ 3.70 GHz,

RAM32.0GB) with a large calculation time more than two months. Note that the similar wave shape can be seen in Figs. 11(b) and 11(c), indicating loosening stopping stage B.

As shown in Fig. 11, the $\theta_L - n$ relation includes several types of local stage denoted by I*, II_F, II_B. As an example, the local stage II_B can be defined where θ_L decreases as $\Delta\theta_L < 0$ contributing the nut tightening instead of the nut loosening. Local stages I*, II_F, II_B observed in the F-n relation will be discussed in detail in the next section.

4.2. Stage I, II, III in F-T relation and local stage I *, II$_F$, II$_B$ in F-n relation

As shown in Figs. 11(b) and 11(c), the local tightening stage II_B can be confirmed as well as the local loosening stage II_F in the F-n relation (clamping force F vs. loading cycle n) in stage B. In the previous study, tightening and untightening the nut were investigated in detail and expressed as the F-T relation (clamping force F vs. torque T). In this section, therefore, the F-n relation will be compared with the F-T relation in terms of nut loosening and the nut tightening.

Figure 12 shows the F-n relation and the F-T relation when $\alpha = 35\,\mu m$ and $\alpha = 40\,\mu m$. Figures 12(a) and 12(c) includes stage A where F decreases, and stage B where F becomes constant. To

Figure 12. F-n relation (Clamping force F vs. loading cycles n relation) explained by F-T relation (a) Clamping force F vs. loading cycles n of $\alpha = 35\,\mu m$; (b) Clamping force F vs. tightening torque T of $\alpha = 35\,\mu m$; (c) Clamping force F vs. loading cycles n of $\alpha = 40\,\mu m$;(d) Clamping force F vs. tightening torque T of $\alpha = 40\,\mu m$.

explain stage A and stage B, the *F-T* relation can be utilized (Noda et al. 2022). As shown in Figs. 12(b) and 12(d), the nut untightening process in the *F-T* relation can be classified into stage I, stage II, and stage III for $\alpha = 35\,\mu$m. Note that the loosening behavior of $\alpha = 35\,\mu$m is totally different from the behavior of $\alpha \geq 40\,\mu$m where there is no stage II. The local stage I *, II_F, II_B in the *F-n* relation can be defined in a similar way of stage I, stage II, and stage III in the *F-T* relation. As already indicated in Fig. 10, the $\theta_L - n$ relation is explained in terms of stages I–III defined as follows.

4.2.1. Stage I in the F-T relation

During stage I in Fig. 12(b), the nut rotates almost together with the bolt. Then, the initial twist energy of the bolt is released as indicated between point G and point G_u in Fig. 12(b). The contact portion of the thread surface and the *F-T* relation are the same irrespective of α. During this stage I, the clamping force *F* almost does not change.

4.2.2. Local stage I * in the F-n relation

Similar to stage I in Fig. 12(b), the Junker type loosening in Fig. 11(a) as well as Fig. 12(a) includes the local stage I * at $n = 0$–0.07 where θ_L increases sharply. In the local stage I *, the bolt and nut rotate completely integrated. For $\alpha = 35\,\mu$m in Figs. 11(a) and 11(b), stage I * can be seen in both stage A and stage B where the bolt and nut are completely integrated and θ_L does not change.

4.2.3. Stage II in the F-T relation

In the *F-T* relation, during this stage II, the nut thread starts slipping from the bolt thread. As shown in Fig. 12(b), $\alpha = 35\,\mu$m has stage II, but as shown in Fig. 12(d), $\alpha = 40\,\mu$m does not have stage II. During stage II for $\alpha = 35\,\mu$m, the contact status from G_u to F_u in Fig. 13 is the same as the one of $\alpha = 0$. Only at F_u in Fig. 13, which is at the end of stage II, both nut ends come into contact with the bolt thread. Therefore, as shown in Fig. 12(b), the *F-T* relation from G_u to F_u is the same for $\alpha = 35\,\mu$m and $\alpha = 0$. Instead, as shown in Fig. 12(d), $\alpha = 40\,\mu$m has no stage II because both nut ends are always in contact with the bolt thread with no status from
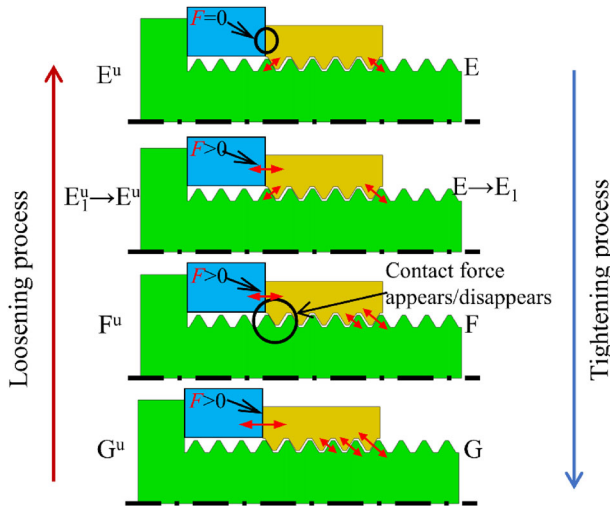

Figure 13. Contact status in tightening and untightening process of nut of $\alpha = 35\,\mu$m.

G_u to F_u in Fig. 13. Therefore, the F-T relation of $\alpha = 40\,\mu$m is always different from that of $\alpha = 35\,\mu$m from the beginning of loosening as shown in Fig. 12(d).

4.2.4. Local stage II_F, II_B in the F-n relation

As shown in Fig. 11, in the F-n relation of the Junker loosening test, there are two local stages; one is the local stage II_F where the nut loosens and the other is the local stage II_B where the nut is tightened. In stage A for $\alpha = 35\,\mu$m in Fig. 11(a), only the local stage II_F can be seen but in stage B for $\alpha = 35\,\mu$m in Figs. 11(b) and 11(c), both of the local stages II_F and II_B can be seen.

4.2.5. Stage III in the F-T relation

As shown in Figs. 12(b) and 12(d), this stage III is the last stage of the F-T relation. During this stage III of $\alpha = 35\,\mu$m, Fig. 13 shows the contact status from F_u to E_u where both ends of the nut contact the bolt threads. Then, the thread contact force at the bearing surface side increases and takes the maximum value when the nut is separated from the clamped body. During this stage III, the bolt axial force between the threads F_α also increases and the clamping force F decreases and finally becomes $F = 0$. Since the thread contact status is different from the status of $\alpha = 0$, the F-T relation is also different as indicated in Fig. 12(b). Then, the clamping force F is hard to decrease since the loosening resistance torque $T_R^u \equiv |T|_{\alpha>0} - |T|_{\alpha=0}$ with $T < 0$ appears (see the Appendix). In this way, stage III contributes to anti-loosening for $\alpha = 35\,\mu$m when the clamping force becomes smaller as $F < 8\,$kN. Therefore, as shown in Fig. 12(b), the anti-loosening effect becomes larger when the initial clamping force $F < 8\,$kN. When $\alpha = 40\,\mu$m, loosening resistance can be expected from the initial stage of loosening because of stage III starts from the beginning of the loosening.

4.3. Loosening progressing stage a and loosening stopping stage B in F-n relation

In Sec. 2.4, from the F-n relation experimentally obtained, stage A was defined as where the loosening is in progress; also, stage B was defined as where the loosening is stopping. In Sec. 4.1, from the F-n relation, the local stage I *, II_F, II_B were discussed; also, from the F-T relation, stage I, II, III were discussed. In this Sec. 4.3, from the θ_L-n relation obtained by FEM, stage A and stage B will be investigated.

As shown in Fig. 11(a), the loosening angle θ_L increases more sharply during $n = 0$–0.05. It should be noted that in the experiment the bolt head may rotate with the nut together by the frictional force, whereas in the FEM simulation the bolt head is fixed. Thus, the loosening angle in at the first stage becomes larger in the simulation. During $n = 0.05$–2, the θ_L-n relations of $\alpha = 0\,\mu$m and $\alpha = 35\,\mu$m can be regarded as stage A where the loosening angle θ_L increases gradually. Stage A is composed of the local stage II_F where θ_L increases and the local stage I^* where θ_L remains constant.

On the other hand, for $\alpha = 40\,\mu$m in Fig. 11(a), stage A can be seen when $n = 0$–0.05, stage B can be seen when $n > 0.05$. In stage B, θ_L is almost constant but the detail observation indicates that stage B of $\alpha = 40\,\mu$m is also composed of the local stage II_F ($\Delta\theta_L > 0$), I^* ($\Delta\theta_L = 0$) and II_B ($\Delta\theta_L < 0$). However, the fluctuation $\Delta\theta_L$ is very smaller compared to that of $\alpha = 0\,\mu$m and $\alpha = 35\,\mu$m. As indicated in Fig. 11(a), Stage A of $\alpha = 35\,\mu$m is composed of the local stage II_F and I^*. Instead, as indicated in Figs. 11(b) and 11(c), stage B of $\alpha = 35\,\mu$m is composed of the local stage II_F, I^*, II_B. In particular, stage B includes II_B where $\Delta\theta_L < 0$. This is the reason why stage B no loosening. In other words, since $\alpha = 0\,\mu$m and $\alpha = 35\,\mu$m in Fig. 11(a) are in stage A without including II_B, nut loosening happens.

Although in Sec. 2.4, stage A and stage B in the F-n relation are defined, they can be redefined in the following way in terms of the θ_L-n relation.

Stage A and stage B in the F-n relation in terms of the θ_L-n relation:

The stage A can be redefined as where consists only of the local stage I^* ($\Delta\theta_L = 0$) and II_F ($\Delta\theta_L > 0$) and therefore the loosening always progresses. Instead, the stage B can be redefined as where the local stage II_F ($\Delta\theta_L > 0$), I^* ($\Delta\theta_L = 0$) and II_B ($\Delta\theta_L < 0$) occur alternately in one vibration cycle and therefore almost no loosening.

4.4. Anti-loosening investigation for pitch difference $\alpha = 35$ μm

Since the F-n relation for $\alpha = 35\,\mu m$ has distinct stage A and Stage B, the anti-loosening property of $\alpha = 35\,\mu m$ will be discussed in detail in this section. Figure 13 compares the experimental results with the FEM simulation results when the vibration cycle $n \leq 302$. In the analysis, as shown in Fig. 6(b), the nut is tightened until the initial tightening force reaches $F = 15\,kN$, which corresponds to 22.3% of the bolt strength. In the experiment, there are a movable plate and a fixed plate as shown in Fig. 3, but in the FEM simulation, the fixed plate is omitted in a similar way as in the previous study (Izumi et al. 2005a)and as shown in Fig. 6(a), the lower side of the bolt head is fixed to the left side of the movable plate (Zhang, Jiang, and Lee 2007). Due to these differences in the boundary condition, both bolt-nut integrated rotation and nut loosening rotation occur in the experiment, but in the analysis, the integrated rotation does not occur, and only the loosening rotation occurs. Therefore, in Fig. 14(a), there are some differences, but the same tendency can be seen. In this FEM simulation, the reduction of F becomes smaller after $n = 50$. Figure 14(b) shows the relation between the vibration cycles and the loosening angle $\theta_L = \theta_N - \theta_B$, the nut rotation angle θ_N and the bolt rotation angle θ_B obtained by FEM when the pitch difference $\alpha = 35\,\mu m$. As shown in Fig. 14(b), the reduction of the loosening angle $\Delta\theta_L$ also becomes smaller after $n = 50$. Figure 14(b) shows that θ_N and θ_L increase in the whole process, whereas θ_B is almost constant except at the beginning of n. Therefore, θ_L almost equals to θ_N as $\theta_L \cong \theta_N$.

Figure 15 shows the details of the nut rotation angle θ_N ($\cong \theta_L$) in Fig. 14(b). Figure 15(a) shows when $n = 0$–2 no local stage II_B ($\Delta\theta_N^{II_B} < 0$) and therefore θ_L increases monotonically. Figure 15(b) may include some local stage II_B ($\Delta\theta_L < 0$) when $n = 10$–12 but the increment $\Delta\theta_N^{II_B}$ is almost zero as $\Delta\theta_N^{II_B} \cong 0$. Instead, Fig. 15(c) shows when $n = 48$–50 the certain local stage II_F but the tightening angle $\Delta\theta_N^{II_B}$ is less than the loosening angle $\Delta\theta_N^{II_F}$ as $\left|\Delta\theta_N^{II_B}\right| < \left|\Delta\theta_N^{II_F}\right|$. Instead, Fig. 15(d) shows when $n = 300$–302 the tightening angle $\Delta\theta_N^{II_B}$ is nearly equal to the loosening angle $\Delta\theta_N^{II_F}$ in one vibration cycle as $\left|\Delta\theta_N^{II_B}\right| \cong \left|\Delta\theta_N^{II_F}\right|$. Figures 15(a)–(d) show with increasing n,
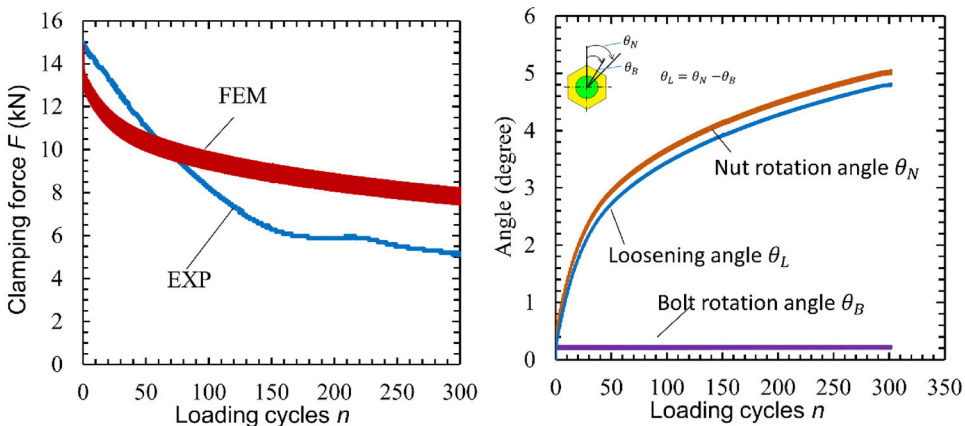

Figure 14. Loosening experiments and analysis for $\alpha = 35$ μm (a) Comparison of F-n relation obtained by FEM and experiment; (b) Nut loosening angles defined as $\theta_L = \theta_N - \theta_B$ obtained by FEM. Here, $\theta_N =$ the nut rotation angle, and $\theta_B =$ the bolt rotation angle.
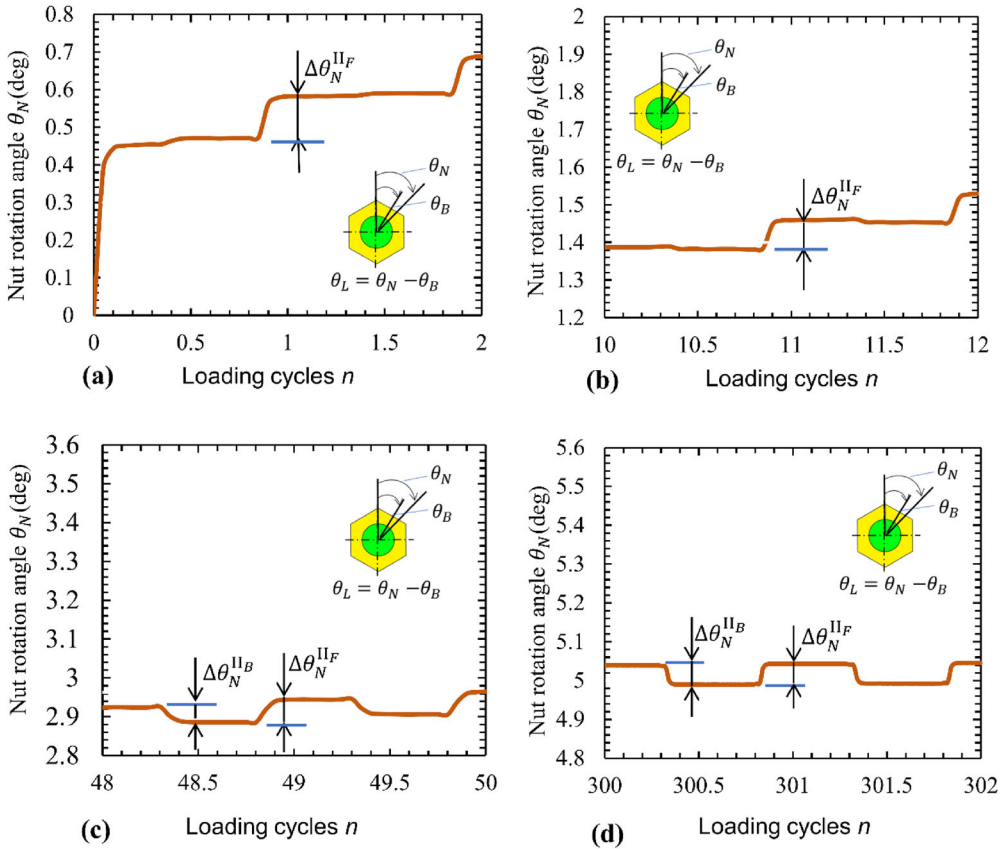
Figure 15. Nut rotation angle θ_N in Figure when (a) n = 0–2, (b) n = 10–12, (c) n = 48–50, (d) n = 300–302.

the amount of tightening angle $|\Delta\theta_L|$ in one cycle increases and approaches the amount of the loosening angle $|\Delta\theta_B|$ in one cycle.

By comparing Fig. 15(a)–(d), it may be concluded that for pitch difference nut the loosening angle $\Delta\theta_N^{II_F}$ in one vibration cycle becomes smaller with increasing n. At the meantime, the tightening angle $\Delta\theta_N^{II_B}$ in one vibration cycle becomes larger with increasing n. Thus, the total loosening angle $(\Delta\theta_N^{II_F} - \Delta\theta_N^{II_B})$ becomes smaller, and decreasing the nut loosening accordingly. Consequently, in $\alpha=35\ \mu m$, as shown in the simulation and experiment, the nut loosening is in progress in the early stage of n as shown in Fig. 14(b), and becoming slower and slower due to the nut both ends contact as shown in F_u in Fig. 13. Then, even under no clamping force $F = 0$ the residual prevailing torque remains (Noda et al. 2020).

5. Conclusions

In the previous studies, the authors verified that a suitable pitch difference nut might improve fatigue strength and anti-loosening at a low cost. In addition, the authors clarified the effect of the pitch difference on the F-T relation to explain the anti-loosening property indirectly. This study aims at confirming the anti-loosening property under real working conditions. JIS M12 bolt-nut connections were treated when the pitch difference $\alpha = 35$, $\alpha = 40$, $\alpha = 50\ \mu m$ in comparison with normal nut $\alpha = 0$. A Junker vibration loosening experiment and a three-dimensional FEM analysis were conducted to investigate the nut loosening mechanism considering the DIN standard demonstrating anti-loosening ability. The effect of pitch difference on the anti-

loosening performance of bolt nut connections is newly discussed when the nut is subjected to a large number of vibrations equivalent to the DIN specifications. The conclusions can be summarized as follows.

1. The Junker's experimental results showed that the pitch difference $\alpha = 40$–50 μm satisfies the DIN25201 anti-loosening standard, which prescribes that the residual clamping force F_u should be larger than 80% of the initial clamping force. Although $\alpha = 35$ μm does not satisfy the DIN standard, $\alpha = 35$ μm sustains a certain amount of the initial clamping force F_u, for example, after the vibration cycle $n = 1500$, F = 4 kN remains, which is 27% of the initial clamping force (see Fig. 4a).
2. Regarding $\alpha = 35$ μm, the F-n relation (clamping force F vs. vibration cycles n) can be classified into the loosening progressing stage A (n $\leq$ 300) and the loosening stopping stage B (n $\geq$ 300). Note that the DIN25201 standard is not suitable for evaluating such peculiar anti-loosening behavior of $\alpha = 35$ μm.
3. In the loosening stopping stage B for $\alpha = 35$–50 μm, the identical waveform can be confirmed. Even in the loosening progressing stage A for $\alpha = 35$ μm, the same waveform also can be seen.
4. Different from $\alpha = 35$–50 μm, all portions of the F-n relation of the normal nut $\alpha = 0$ belong to stage A and no portion belongs to stage B. Compared to $\alpha = 0$, the generation mechanism of stage B for $\alpha = 35$–50 μm was clarified from the thread contact force and slip (see Fig. 11).
5. The peculiar anti-loosening behavior of $\alpha = 35$ μm in the F-n relation can be explained from the F-T relation (clamping force F vs. tightening torque T) discussed in the previous studies. Only at the end of the nut loosening process, denoted as stage III, both ends of the nut contact the bolt thread. Due to this thread contact, the loosening resistance torque becomes larger when the clamping force F < 8 kN as shown in Fig. 12(b). Then, the loosening stopping stage B appears for $\alpha = 35$ μm in the F-n relation when $n \geq 300$.
6. The θ_L-n relation (loosening angle θ_L vs. vibration cycle n) was investigated through the FEM analysis. The loosening progressing stage A consists of the local stage I* where the loosening angle in one vibration cycle $\Delta\theta_L = 0$ and the local stage II$_F$ where $\Delta\theta_L > 0$. This is the reason why the loosening always progresses in sage A. Instead, the loosening stopping stage B consists of three local stages II$_F$ $(\Delta\theta_L > 0)$, I* $(\Delta\theta_L = 0)$ and II$_B$ $(\Delta\theta_L < 0)$ in one vibration cycle. Due to the local stage II$_B$ $(\Delta\theta_L < 0)$, almost no loosening in stage B.
7. During stage A ($n \leq 300$), with increasing n, the loosening angle in one cycle decreases and the tightening angle in one cycle increases. Then, during stage B ($n \geq 300$), the loosening angle is equal to the tightening angle in one loading cycle and therefore no loosening.

Acknowledgments

References

Barrett, R. T. 1990. *NASA reference publication 1228*. Fastener Design Material, NASA, Office of Management, Scientific and Technical Information Division.

Bhattacharya, A., A. Sen, and S. Das. 2010. An investigation on the anti-loosening characteristics of threaded fasteners under vibratory conditions. *Mechanism and Machine Theory*.45 (8):1215–25. doi:10.1016/j.mechmachtheory.2008.08.004.

Chen, D., E. Shimizu, and K. Masuda. 2012. Relation between thread deformation and anti-loosening effect for nut with circumference slits. *Transactions of the Japan Society of Mechanical Engineers Series A* 78 (788):390–402. doi:10.1299/kikaia.78.390.

Chen, X., N. A. Noda, M. A. Wahab, Y. Sano, H. Maruyama, H. Wang, R. Fujisawa, and Y. Takase. 2016. Fatigue life improvement by slight pitch difference in bolt-nut connections. *Journal of the Chinese Society of Mechanical Engineers, Series C: Transactions of the Chinese Society of Mechanical Engineers* 37:11–9.

Eccles, W., I. Sherrington, and R. D. Arnell. 2010. Towards an understanding of the loosening characteristics of prevailing torque nuts. *Proceedings of the Institution of Mechanical Engineers, Part C: Journal of Mechanical Engineering Science* 224 (2):483–95. doi:10.1243/09544062JMES1493.

Eccles, W. S. 2010. *Tribological aspects of the self-loosening of threaded fasteners*. Doctoral dissertation, University of Central Lancashire.

Gong, H., J. Liu, and X. Ding. 2021. Study on local slippage accumulation between thread contact surfaces and novel anti-loosening thread designs under transversal vibration. *Tribology International* 153:106558. doi:10.1016/j.triboint.2020.106558.

Gong, H., J. Liu, and H. Feng. 2022. Review on anti-loosening methods for threaded fasteners. *Chinese Journal of Aeronautics* 35 (2):47–61. doi:10.1016/j.cja.2020.12.038.

HARDLOCK Industry Co. Ltd. 2022. Junker type screw loosening test - test data [WWW document]. https://hard-lock.co.jp/technical-info/data/junker-test/. Accessed June 18, 2022.

Hirai, K., and N. Uno. 2005. Fatigue strength of super high strength bolt. *Journal of Structural and Construction Engineering (Transactions of AIJ)* 70 (595):117–22. doi:10.3130/aijs.70.117_2.

Izumi, S., T. Yokoyama, A. Iwasaki, and S. Sakai. 2005a. Three-dimensional finite element analysis of tightening and loosening mechanism of threaded fastener. *Engineering Failure Analysis* 12 (4):604–15. doi:10.1016/j.engfailanal.2004.09.009.

Izumi, S., T. Yokoyama, M. Kimura, and S. Sakai. 2009. Loosening-resistance evaluation of double-nut tightening method and spring washer by three-dimensional finite element analysis. *Engineering Failure Analysis* 16 (5):1510–9. doi:10.1016/j.engfailanal.2008.09.027.

Izumi, S., T. Yokoyama, T. Teraoka, A. Iwasaki, S. Sakai, K. Saito, M. Nagawa, and H. Noda. 2005b. Verification of anti-loosening performance of super slit nut BV finite element method. *Transactions of the Japan Society of Mechanical Engineers Series A* 71 (703):380–6. doi:10.1299/kikaia.71.380.

Liu, J., H. Gong, and X. Ding. 2018. Effect of ramp angle on the anti-loosening ability of wedge self-locking nuts under vibration. *Journal of Mechanical Design* 140 (7):072301. doi:10.1115/1.4040167.

Liu, X., B. Wang, N.-A. Noda, Y. Sano, Y. Inui, K. Tateishi, and Y. Takase. 2021. Bolt clamping force versus torque relation (F-T relation) during tightening and untightening the nut having slight pitch difference. *Mechanics Based Design of Structures and Machines*: 1–18. doi:10.1080/15397734.2021.1931308.

Majzoobi, G. H., G. H. Farrahi, and N. Habibi. 2005. Experimental evaluation of the effect of thread pitch on fatigue life of bolts. *International Journal of Fatigue.*27 (2):189–96. doi:10.1016/j.ijfatigue.2004.06.011.

Nishiyama, S., H. Migita, M. Kataoka, N. Nakasaki, and K. Murano. 2009. Development of anti-loosening performance of hyper lock nut. *Journal of System Design and Dynamics* 3 (1):147–61. doi:10.1299/jsdd.3.147.

Noda, N. A., X. Chen, Y. Sano, M. A. Wahab, H. Maruyama, R. Fujisawa, and Y. Takase. 2016. Effect of pitch difference between the bolt–nut connections upon the anti-loosening performance and fatigue life. *Materials and Design.*96:476–89. doi:10.1016/j.matdes.2016.01.128.

Noda, N.-A., M. Kuhara, Y. Xiao, S. Noma, K. Saito, M. Nagawa, A. Yumoto, and A. Ogasawa. 2008a. Stress reduction effect and anti-loosening performance of outer cap nut by finite element method. *Journal of Solid Mechanics and Materials Engineering* 2 (6):801–11. doi:10.1299/jmmp.2.801.

Noda, N.-A., X. Liu, Y. Sano, K. Tateishi, B. Wang, Y. Inui, and Y. Takase. 2022. Prevailing torque and residual prevailing torque of Bolt-Nut connections having slight pitch difference. *Mechanics Based Design of Structures and Machines* 50 (6):2032–45. doi:10.1080/15397734.2020.1768114.

Noda, N.-A., X. Liu, Y. Sano, K. Tateishi, B. Wang, and Y. Takase. 2020. Three-dimensional finite element analysis for prevailing torque of bolt-nut connection having slight pitch difference. *Journal of Mechanical Science and Technology* 34 (6):2469–76. doi:10.1007/s12206-020-0522-8.

Noda, N.-A., B. Wang, K. Oda, Y. Sano, X. Liu, Y. Inui, and T. Yakushiji. 2021. Effects of root radius and pitch difference on fatigue strength and anti-loosening performance for high strength bolt–nut connections. *Advances in Structural Engineering* 24 (9):1941–54. doi:10.1177/1369433220988619.

Noda, N.-A., Y. Xiao, and M. Kuhara. 2011. The reduction of stress concentration by tapering threads. *Journal of Solid Mechanics and Materials Engineering* 5 (8):397–408. doi:10.1299/jmmp.5.397.

Noda, N.-A., Y. Xiao, M. Kuhara, K. Saito, M. Nagawa, A. Yumoto, and A. Ogasawara. 2008b. Optimum design of thin walled tube on the mechanical performance of super lock nut. *Journal of Solid Mechanics and Materials Engineering* 2 (6):780–91. doi:10.1299/jmmp.2.780.

Pai, N. G., and D. P. Hess. 2002. Experimental study of loosening of threaded fasteners due to dynamic shear loads. *Journal of Sound Vibrations.*253 (3):585–602. doi:10.1006/jsvi.2001.4006.

Pai, N. G., and D. P. Hess. 2004. Dynamic loosening of threaded fasteners. *Noise & Vibration Worldwide* 35 (2):13–9. doi:10.1260/0957456041217298.

Panja, B., and S. Das. 2016. Antiloosening ability of 5/8 inch stainless steel BSW threaded fasteners. *AIP Conference Proceedings* 1754, 030015. doi:10.1063/1.4958359.

Panja, B., and S. Das. 2017. Development of an anti-loosening fastener and comparing its performance with different other threaded fasteners. *Sādhanā* 42 (10):1793–801. doi:10.1007/s12046-017-0719-4.

Ranjan, B. S. C., H. N. Vikranth, and A. Ghosal. 2013. A novel prevailing torque threaded fastener and its analysis. *Journal of Mechanical Design* 135 (10):101007. doi:10.1115/1.4024977.

Samanta, S., S. Das, R. Roy, K. Bhukta, A. Pal, and S. Das. 2012. Comparison of loosening characteristics of 3/8 BSW threaded fasteners under accelerated vibratory condition. *Journal of the Association of Engineers, India* 82 (3–4):34–43. doi:10.22485/jaei/2012/v82/i3-4/119938.

Sawa, S., M. Ishimura, Y. Sekiguchi, and T. Sawa. 2015. *3-D FEM stress analysis and mechanical characteristics in bolted joints under external tensile loadings.* Proceedings of the ASME 2015 International Mechanical Engineering Congress and Exposition. Houston, Texas, USA, 1–9. doi:10.1115/IMECE2015-50572.

Sawa, T., M. Ishimura, and H. Yamanaka. 2006. Experimental evaluation of screw thread loosening in bolted joint with some parts for preventing the loosening under transverse repeated loadings. doi:10.1115/PVP2006-ICPVT-11-93292.

Shoji, Y., T. Sawa, and H. Yamanaka. 2007. Self-loosening mechanism of nuts due to lateral motion of fastened plate. doi:10.1115/PVP2007-26409.

Wakabayashi, K. 2002. Hard lock nut. Japanese Patent.

Wang, B., N. A. Noda, X. Liu, Y. Sano, Y. Inui, and K. Oda. 2021. How to improve both anti-loosening performance and fatigue strength of bolt nut connections economically. *Engineering Failure Analysis* 130:105762. doi:10.1016/j.engfailanal.2021.105762.

Xin, C., N. Nao-Aki, W. M. Abdel, A. Yu-Ichiro, S. Yoshikazu, T. Yasushi, and F. Gusztav. 2015. Fatigue failure analysis for bolt-nut connections having slight pitch differences using experimental and finite element methods. *Acta Polytechnica Hungarica* 12 (8):61–79. doi:10.12700/aph.12.8.2015.8.4.

Yang, B., Q. Sun, Q. Lin, L. Wang, X. Zhang, and Y. Ma. 2021. Influence mechanism of bolted joint with geometric irregularity bearing surface on anti-loosening performance. *International Journal of Pressure Vessels and Piping* 191:104364. doi:10.1016/j.ijpvp.2021.104364.

Yang, L., B. Yang, G. Yang, Y. Xu, S. Xiao, S. Jiang, and J. Chen. 2021. Analysis of competitive failure life of bolt loosening and fatigue. *Engineering Failure Analysis* 129:105697. doi:10.1016/j.engfailanal.2021.105697.

You, J. M., Y. C. Hong, S. H. Jeon, J. Huh, and J. H. Ahn. 2020. Behavior of bolt-connected steel plate girder attributable to bolt loosening failure in the lower flange. *Engineering Failure Analysis* 107:104208. doi:10.1016/j.engfailanal.2019.104208.

Zhang, M., Y. Jiang, and C.-H. Lee. 2007. Finite element modeling of self-loosening of bolted joints. *Journal of Mechanical Design* 129 (2):218–26. doi:10.1115/1.2406092.

Zhang, M., L. Lu, W. Wang, and D. Zeng. 2018. The roles of thread wear on self-loosening behavior of bolted joints under transverse cyclic loading. *Wear* 394–395:30–9. doi:10.1016/j.wear.2017.10.006.

Zhou, J., J. Liu, H. Ouyang, Z. Cai, J. Peng, and M. Zhu. 2018. Anti-loosening performance of coatings on fasteners subjected to dynamic shear load. *Friction* 6 (1):32–46. doi:10.1007/s40544-017-0160-z.

Appendix: *F-T relations for pitch difference nut with the definition of T_p, T_{slip}, T_R^u, T_p^u, $\tilde{T}_R^u$*

Figure A1 illustrates the screwing, tightening, untightening and unscrewing the pitch difference nut. Those processes were studied experimentally and analytically by using FEM (Liu et al. 2021; Noda et al. 2022, 2020; Wang et al. 2021). Figure A2 illustrates the *F-T* relation (the clamping force *F* vs. the tightening torque *T*) for $\alpha = 45\,\mu m$ and $H = 10.5\,mm$ obtained by FEM analysis. The green line of $\alpha = 45\,\mu m$ is compared with the gray line of $\alpha = 0$. For example, Fig. A2(b) shows the *F-T* relation during the nut position changed as E → F→G→G_u → F_u→E_u in Fig. A1(e).

The clamping force *F* appears by applying $T > 0$ for $\alpha = 0$. Instead, the clamping force *F* of $\alpha = 45$ μm appears by applying $T \geq T_P$ when the torque exceeds the prevailing torque T_P. The prevailing torque T_P can be defined in Eq. (A.1) at *E* in Fig. A1(e).

$$T_P \equiv \sup T \quad when \ F = 0, \ T > 0 \tag{A.1}$$

With increasing $T \geq T_p$, the clamping force *F* increases. When $T = T_{25\%}$ or $T = T_{50\%}$, *F* becomes largest as $F = F_{max}$ at F in Fig. A1(e) as shown in Eq. (A.2).

$$F_{max} \equiv \text{Max}|F| \quad when \ T = T_{25\%} \ or \ T = T_{50\%} \tag{A.2}$$

Here, $T_{25\%} = 45Nm$ is the torque *T* producing $F = F_{25\%} = 16.8KN$ for $\alpha = 0$ and $T_{50\%} = 85Nm$ is the torque *T* producing $F = F_{50\%} = 33.8KN$ for $\alpha = 0$. It should be noted that $F = F_{max}$ varies depending on α.
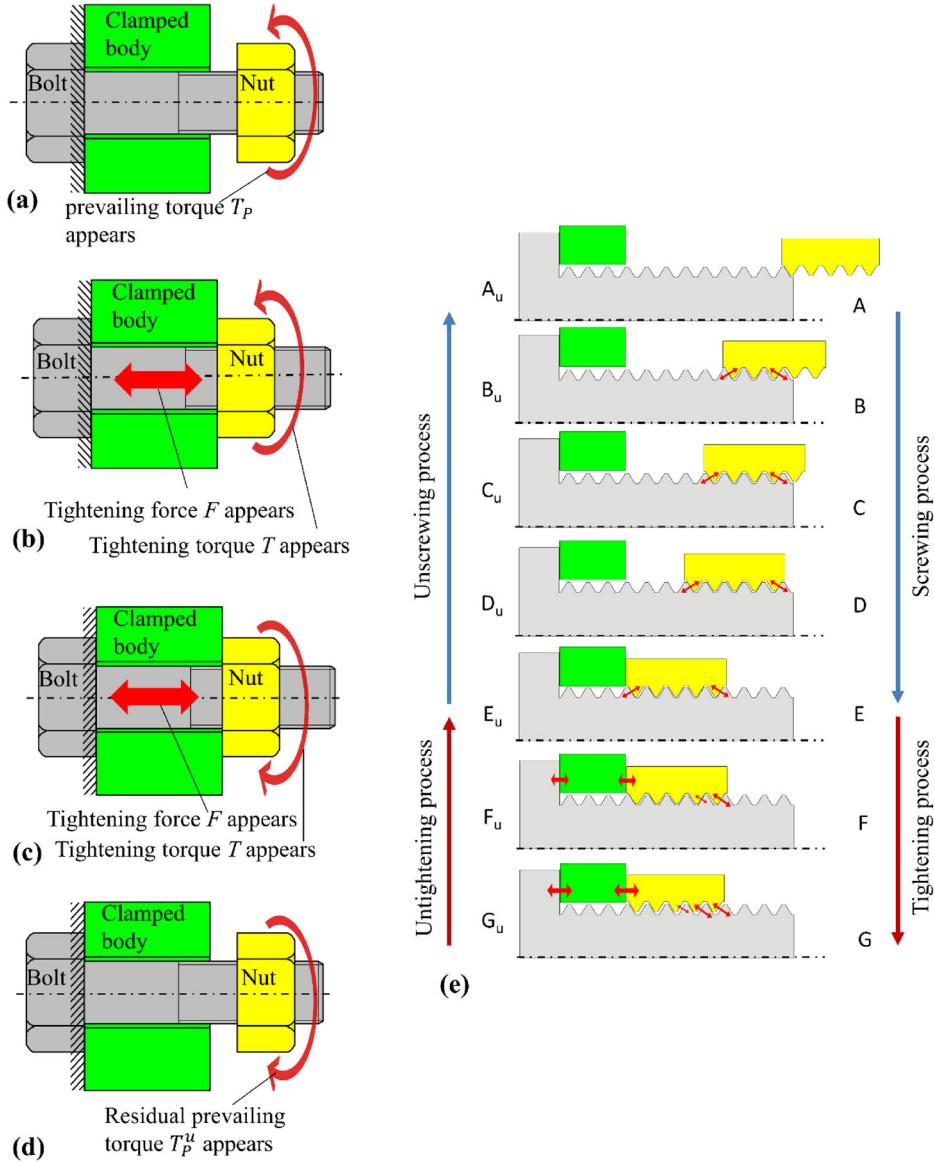
Figure A1. Illustration for (a) Screwing process; (b) Tightening process; (c) Untightening process; (d) Unscrewing process and (e) Tread contact status change when the nut position is changed as A→B→ … →F→G→Gu→Fu→ … →Bu→Au.

After T reaches $T = T_{25\%}$ or $T = T_{50\%}$, untightening torque is applied as $T < 0$. Initially, F is almost constant as $F \approx F_{max}$ since the bolt-nut rotates together. After $|T|$ reaches the slip torque T_{slip} defined in Eq. (A.3), the nut rotates independently. Then, F starts decreasing with decreasing $|T|$ as $F < F_{max}$ from Point G_u in Fig. A2(b).

$$T_{slip} \equiv \text{Max } |T| \text{ when } T < 0 \text{ after } T = T_{25\%} \text{ or } T = T_{50\%} \tag{A.3}$$

As shown in $G_u \to F_u$ in Fig. A2, during F decreasing under untightening $T < 0$, initially the F-T relations are equal for $\alpha = 45\,\mu m$ and $\alpha = 0$. During $F_u \to E_u$ in Fig. A1, the light green zone illustrates the difference between $\alpha = 0$ and $\alpha = 45\,\mu m$. The difference can be considered as a loosening resistance torque T_R^u contributing to anti-loosening, which is defined in Eq. (A.4) (Liu et al. 2021).

$$T_R^u \equiv |T|_{\alpha > 0} - |T|_{\alpha = 0} \text{ when } T < 0, \tag{A.4}$$
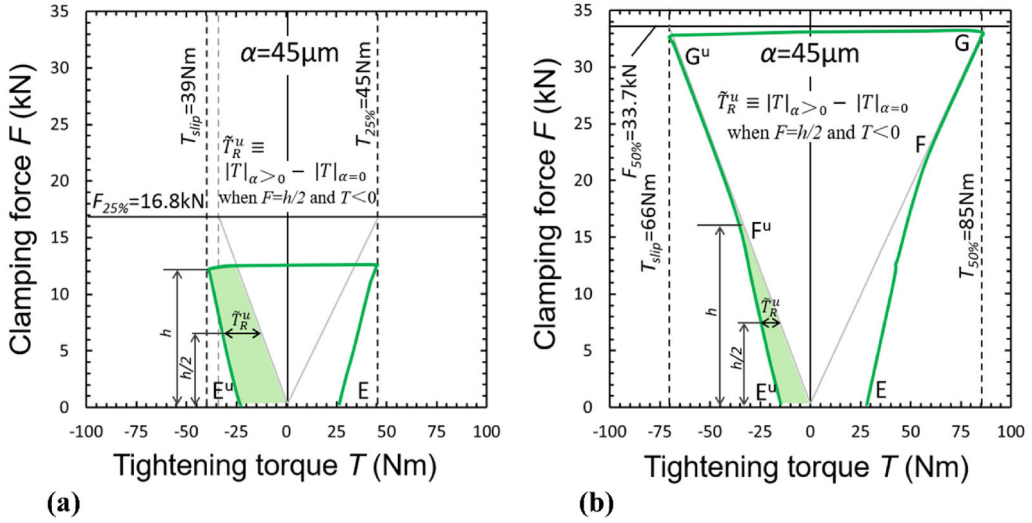$$T_R^u > 0 \text{ when } 0 \leq F < h, \text{ i.e. } h \equiv \sup F \text{ when } T_R^u > 0$$

Figure A2. Relation between the clamping force F and the tightening torque T: (a) when $\alpha = 45\ \mu m$ under $T \leq T_{25\%} = 45$ Nm; (b) when $\alpha = 45\ \mu m$ under $T \leq T_{50\%} = 80$ Nm.

At E_u in Fig. A2, even no tightening force $F = 0$, $T_R^u > 0$. Therefore, the loosening resistance torque T_R^u can be characterized at the value when $F = 0$. The value T_R^u at $F = 0$ can be named the residual prevailing torque and defined in Eq. (A.5).

$$T_P^u \equiv T_R^u \ \ when \ F = 0 \tag{A.5}$$

The residual prevailing torque T_P^u above may represent the anti-loosening performance (Liu et al. 2021; Noda et al. 2022; Wang et al. 2021). However, T_R^u is changing during $F_u \rightarrow E_u$. Therefore, the median loosening resistance torque can be considered and defined in Eq. (A.6).

$$\tilde{T}_R^u \equiv |T|_{\alpha > 0} - \ |T|_{\alpha = 0} \ \ when \ F = h/2 \ and \ T < 0 \tag{A.6}$$

The median loosening resistance torque may represent T_R^u variation during $F_u \rightarrow E_u$.

$$Regarding \ the \ normal \ nut \ \alpha = 0, \ \ T_P = T_R^u = T_P^u = \tilde{T}_R^u = 0 \qquad \qquad .$$